Supporting information for:

Photo-initiated oxidation of C–H bonds by diimine complexes of vanadium(V)

Rui Zhang and Jeffrey J. Warren

Simon Fraser University, Chemistry, 8888 University Drive, Burnaby, BC V5A 1S6, Canada

Contents

Materials and methods 2
Synthetic scheme for $V^{V}(O)(O)$ and $V^{V}(O)(O_2)$ compounds 2
Luminescence spectra for $V^{V}(O)(O)$ and $V^{V}(O)(O_2)$ 3
^{1}H NMR spectra for DHA and oxidation products 4
^{1}H NMR spectra for xanthene and oxidation products 5
^{1}H NMR spectra for fluorene and oxidation products 6
^{1}H NMR spectra for triphenylmethane (Ph_3CH) and oxidation products 7
^{1}H NMR spectra for toluene and oxidation products 8
Yields and product distribution for different substrates 9
X-ray crystallography 9
Crystal structure of compound 1 (9,9′,10,10′-tetrahydro-9,9′-bianthracene) 10
Crystal structure of compound 2 (bianthronyl) 10
Crystal structure of compound 3 (anthraquinone) 11
^{1}H NMR spectra for the reaction of toluene with $V^{V}(O)(O)$ under air and N_2 11
^{1}H NMR spectra for reaction of DHA with $V^{V}(O)(O)$ under air and N_2 12
Comparison of photochemical oxidations using different ratios of V-complexes and DHA under N_2 and O_2 12
^{51}V NMR spectra for $V^{V}(O)(O)$ before and after irradiation under O_2, air and N_2 13
^{51}V NMR spectra for $V^{V}(O)(O_2)$ before and after photochemical reaction under O_2, air and N_2 . 13
^{1}H NMR spectra for $V^{V}(O)(O)$ before and after photochemical reaction under O_2, air and N_2 ... 14
^{1}H NMR spectra for $V^{V}(O)(O_2)$ before and after photochemical reaction under O_2, air and N_2 .. 15
IR spectra for $V^{IV}(O)(OH)$, $V^{V}(O)(O)$ and $V^{V}(O)(O_2)$ 16
IR spectra for $V^{V}(O)(O)$ before and after photochemical reaction under O_2, air and N_2 16
IR spectra for $V^{V}(O)(O_2)$ before and after photochemical reaction under O_2, air and N_2 17
UV-vis spectra for $V^{IV}(O)(OH)$, $V^{V}(O)(O)$ and $V^{V}(O)(O_2)$ 17
UV-vis spectra for $V^{V}(O)(O)$ before and after photochemical reaction under O_2, air and N_2 18
UV-vis spectra for $V^{V}(O)(O_2)$ before and after photochemical reaction under O_2, air and N_2 18
Computational Details 19
References 21

Materials and methods

All chemicals were purchased from Sigma-Aldrich and were used as received, unless noted otherwise. Solvents were from J.T. Baker. Gases were got from Praxair Canada. All vanadium complexes were prepared (see below) and characterized following literature procedures.[1,2] Nuclear magnetic resonance (NMR) was carried out using the Bruker Ultrashield^{TM} 400 plus. The photochemical character was studied using Spectrofluorometer FS5 (Edinburgh Instruments Ltd). UV-visible (UV-vis) spectra were collected using a Cary100Bio UV-vis spectrophotometer. FT-IR was tested using NEXUS 670 FT-IR of Thermo Instruments (Canada) Inc.

Synthetic scheme for $V^{V}(O)(O)$ and $V^{V}(O)(O_2)$ compounds

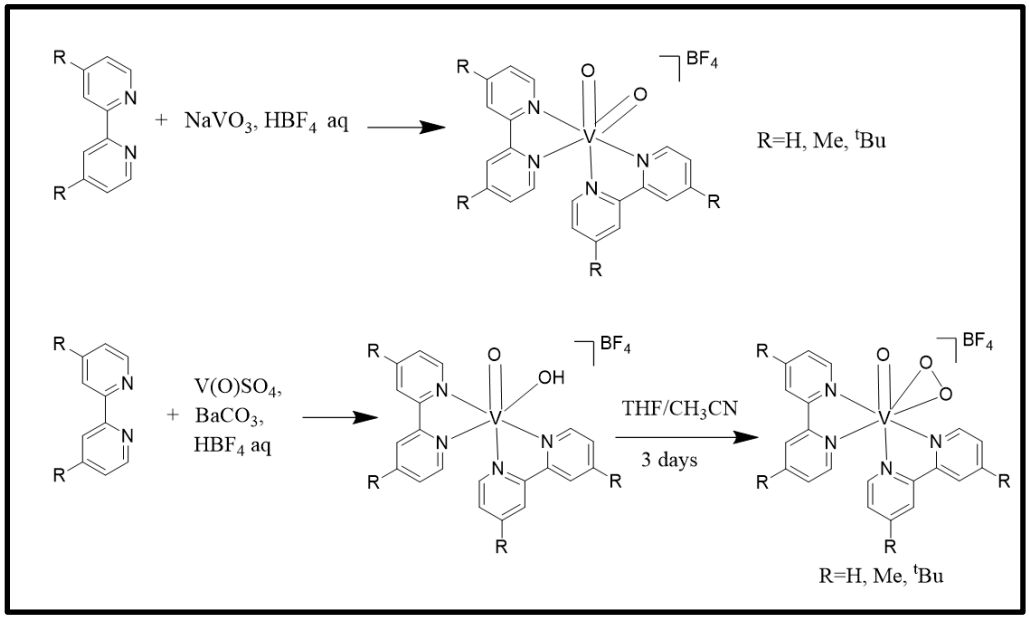

Figure S1. The syntheses of $V^{V}(O)(O)$ and $V^{V}(O)(O_2)$ compounds.

Luminescence spectra for $V^{V}(O)(O)$ and $V^{V}(O)(O_2)$

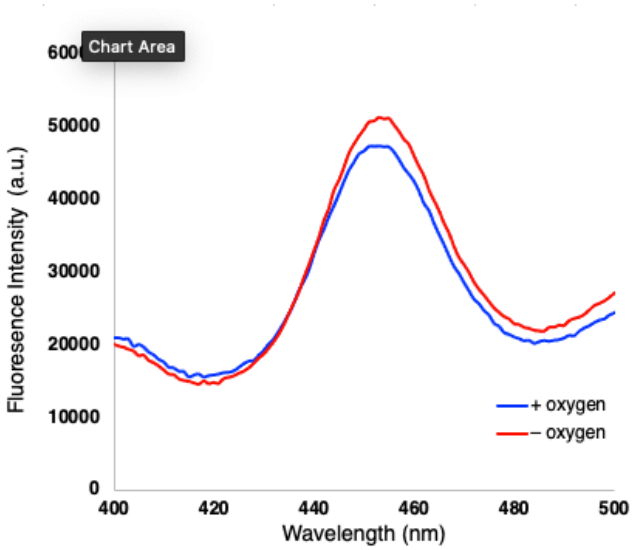

Figure S3. Photoluminescence spectra for $V^{V}(O)(O)$ in the presence (blue trace) and absence (red trace) of O_2.

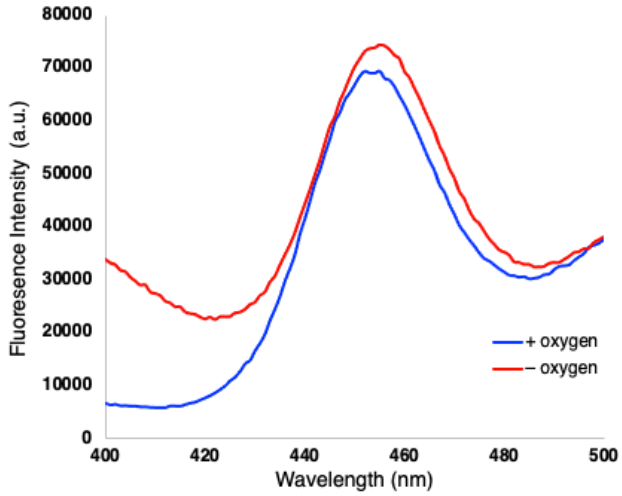

Figure S3. Photoluminescence spectra for $V^{V}(O)(O_2)$ in the presence (blue trace) and absence (red trace) of O_2.

^{1}H NMR spectra for DHA and oxidation products

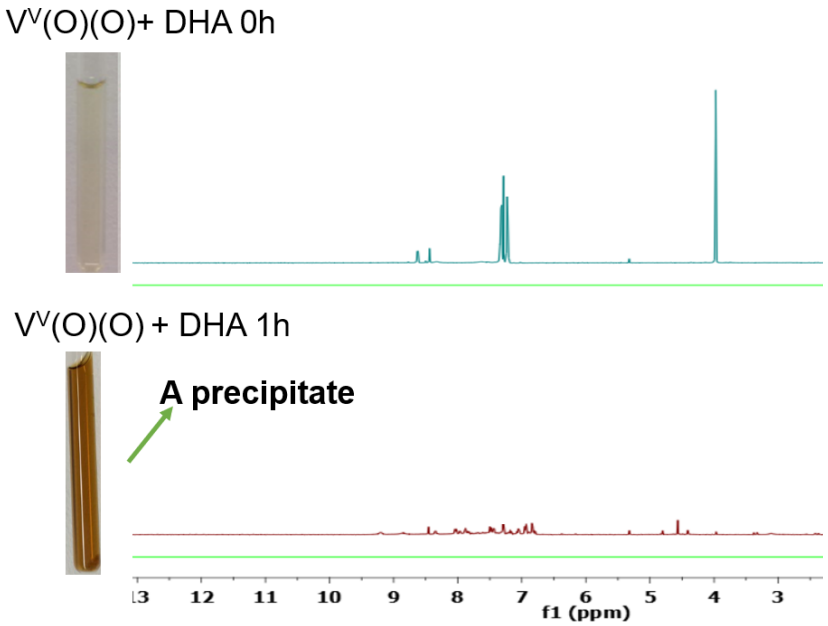

Figure S4. Before and after 60 min irradiation ^{1}H NMR spectra for a solution of DHA and V^V(O)(O) in CD_3CN (green was before reaction and red was after reaction). Images of the NMR tubes before and after reactions are shown at left.

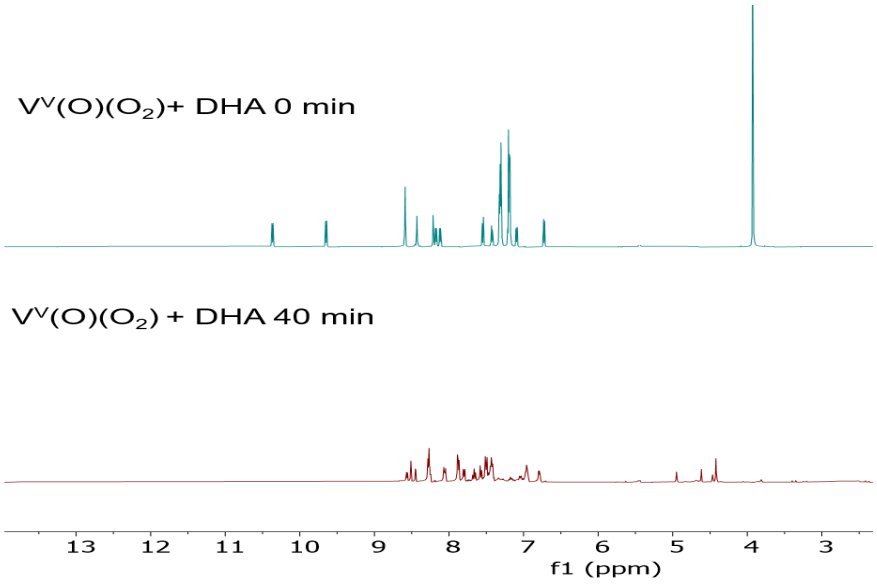

Figure S5. Before and after 40 min irradiation ^{1}H NMR spectra for a solution of DHA and V^V(O)(O_2) in CD_3CN (green was before reaction and red was after reaction).

^{1}H NMR spectra for xanthene and oxidation products

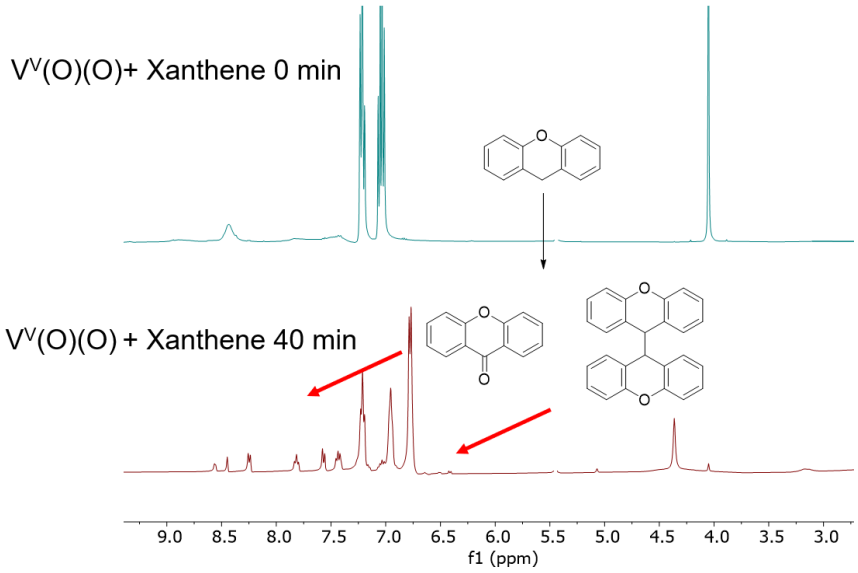

Figure S6. Before and after 40 min irradiation ^{1}H NMR spectra for a solution of xanthene V^V(O)(O) in CD_3CN (green was before reaction and red was after reaction).

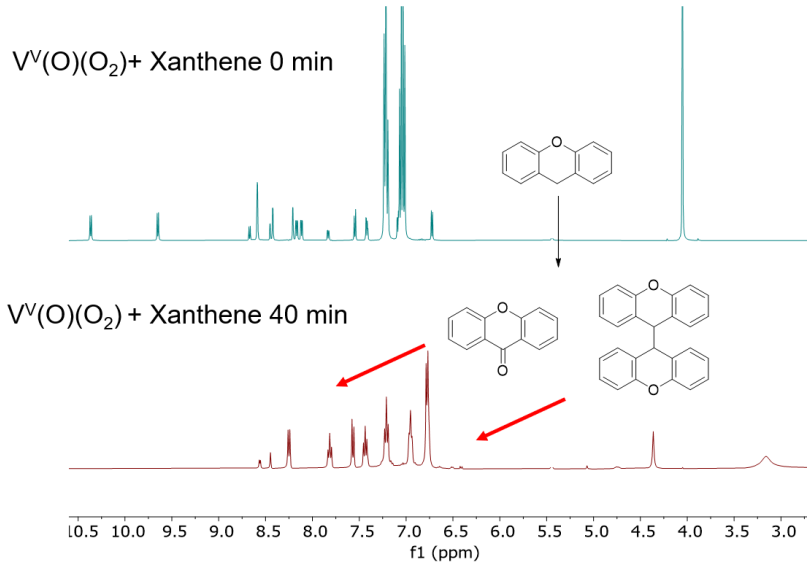

Figure S7. Before and after 40 min irradiation ^{1}H NMR spectra for a solution of xanthene and V^V(O)(O$_2$) in CD_3CN (green was before reaction and red was after reaction).

^{1}H NMR spectra for fluorene and oxidation products

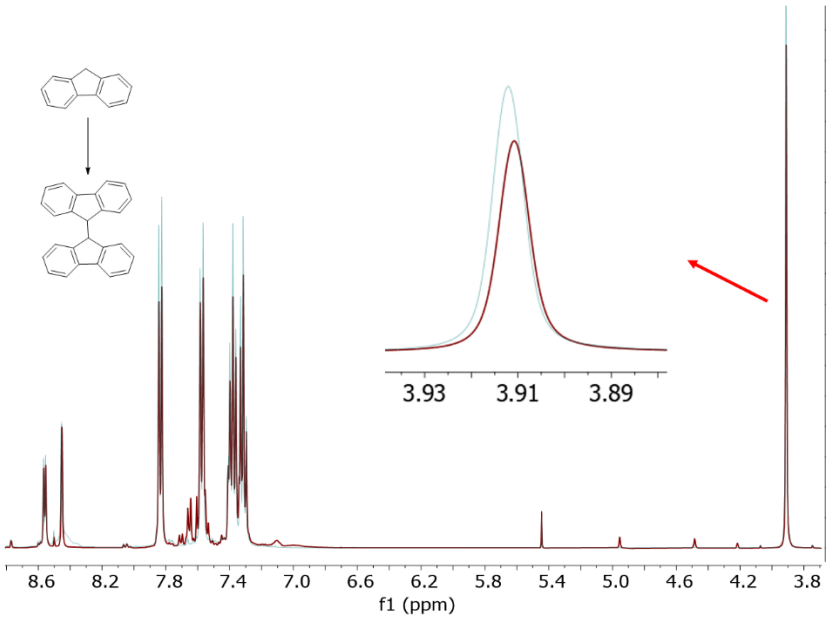

Figure S8. Before and after 240 min irradiation ^{1}H NMR spectra for a solution of fluorene and $V^V(O)(O)$ in CD_3CN (green was before reaction and red was after reaction).

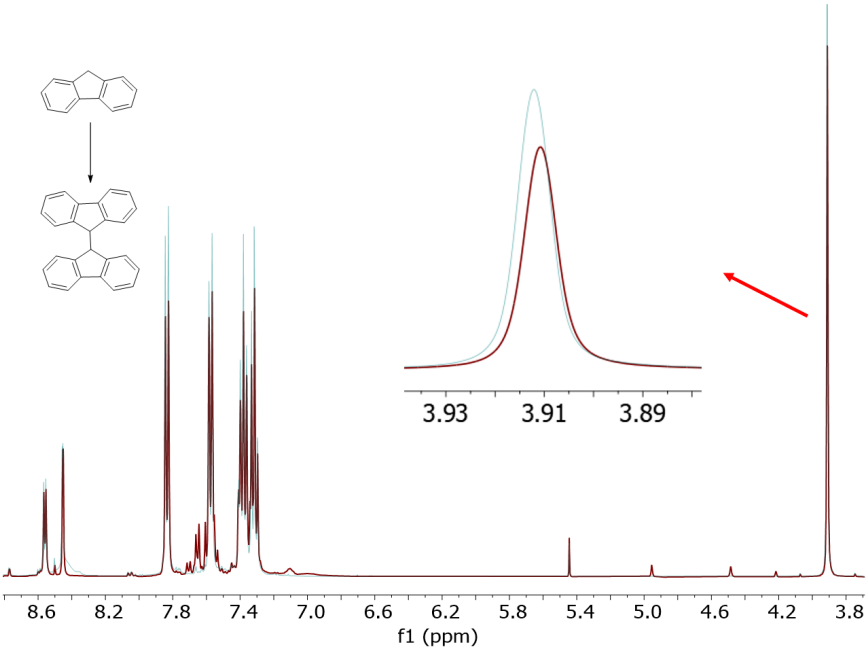

Figure S9. Before and after 240 min irradiation ^{1}H NMR spectra for a solution of fluorene and $V^V(O)(O_2)$ in CD_3CN (green was before reaction and red was after reaction).

^{1}H NMR spectra for triphenylmethane (Ph_3CH) and oxidation products

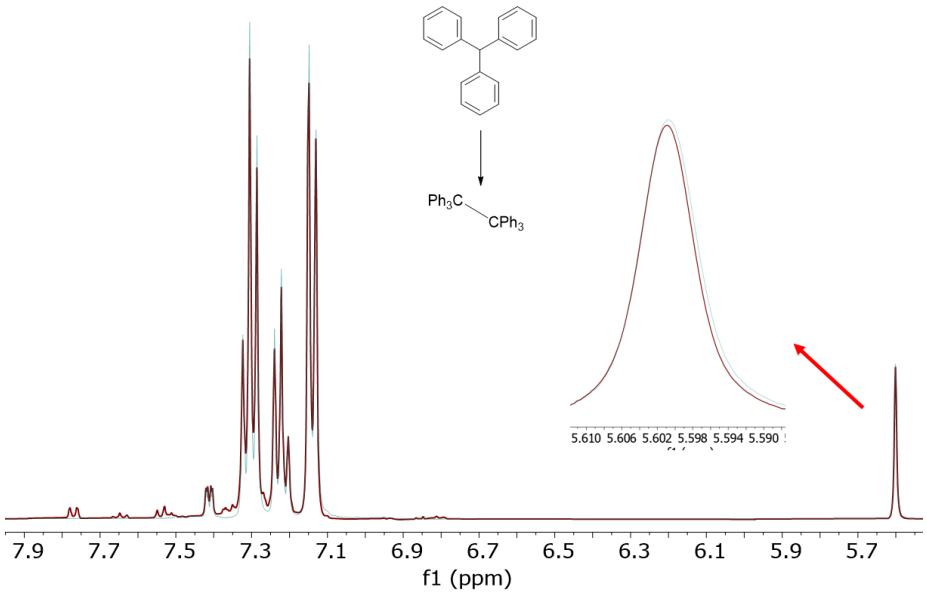

Figure S10. Before and after 360 min irradiation ^{1}H NMR spectra for a solution of Ph_3CH and $V^V(O)(O)$ in CD_3CN (green was before reaction and red was after reaction).

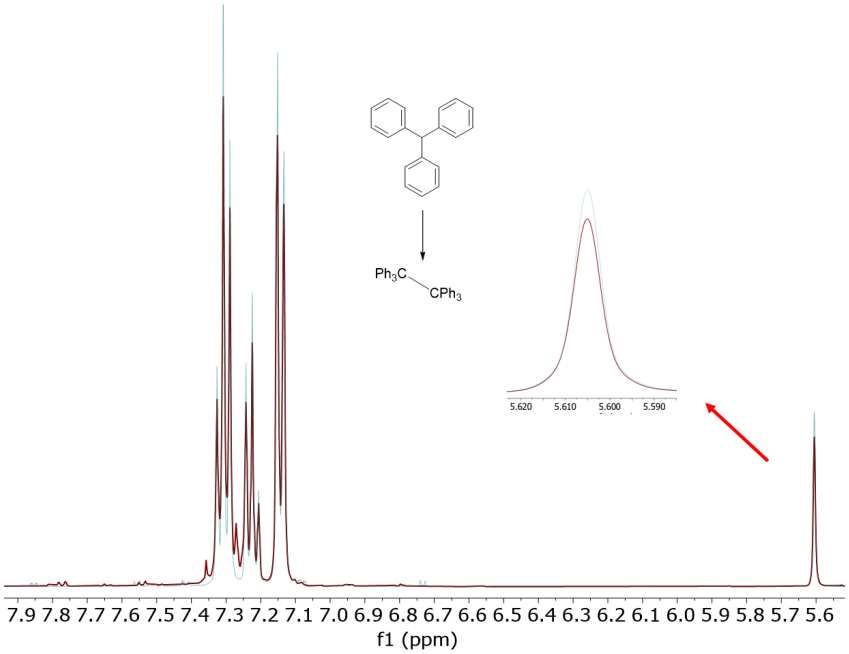

Figure S11. Before and after 360 min irradiation ^{1}H NMR spectra for a solution of Ph_3CH and $V^V(O)(O_2)$ in CD_3CN (green was before reaction and red was after reaction).

^{1}H NMR spectra for toluene and oxidation products

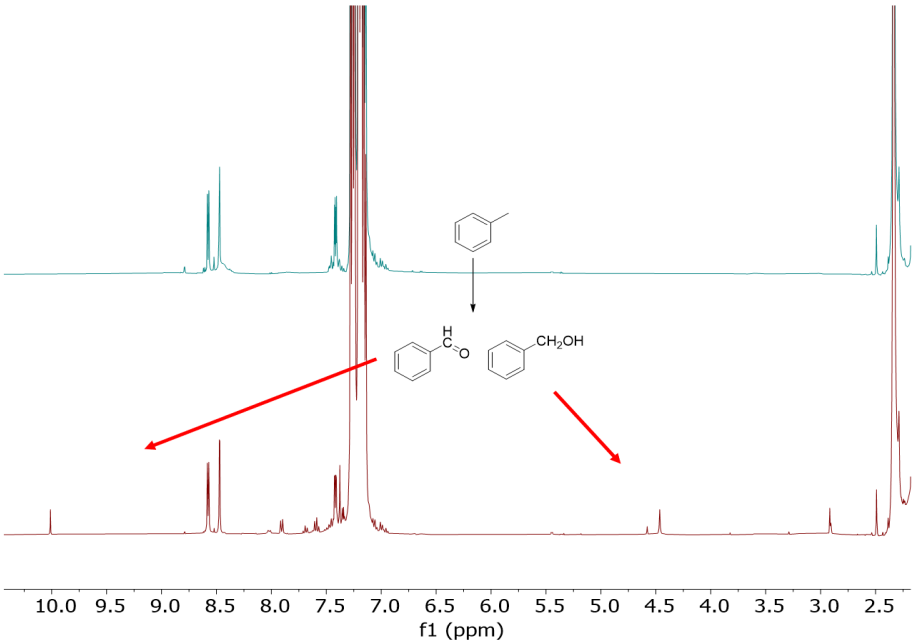

Figure S12. Before and after 540 min irradiation ^{1}H NMR spectra for a solution of toluene and $V^V(O)(O)$ in CD_3CN (green was before reaction and red was after reaction).

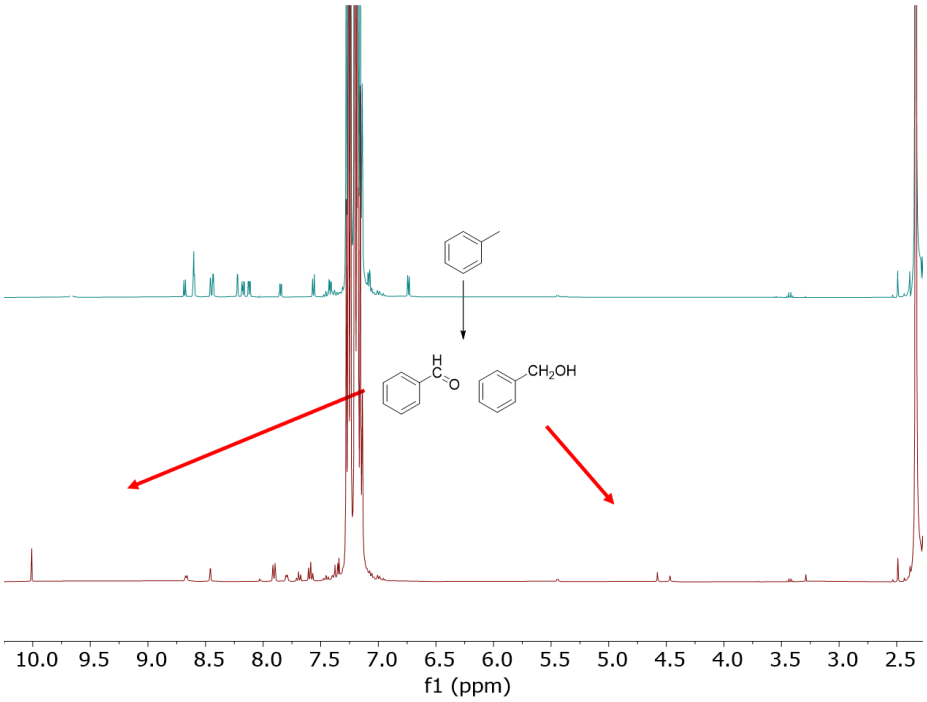

Figure S13. Before and after 540 min irradiation ^{1}H NMR spectra for a solution of toluene and $V^V(O)(O_2)$ in CD_3CN (green was before reaction and red was after reaction).

Yields and product distribution for different substrates

Table S1. Yields and product distribution for different substrates using V(O)(O) or V(O)(O_2) calculated from ^{1}H NMR integration.

Substrates	Product	Relative Yield w/ V(O)(O) (%)	Relative Yield w/ V(O)(O_2) (%)
Xanthene	dixanthene	94	88
	xanthone	6	12
9,10	bianthracene	88	76
dihydroanthracene	bianthronyl	6	11
	anthraquinone	6	14
fluorene	dimer	100	100
triphenylmethane	dimer	100	100
toluene	phenylethanol	71	29
	benzaldehyde	34	67

X-ray crystallography

Crystals were coated in paratone oil, mounted on a MiTeGen Micro Mount. Data were collected on a Bruker Smart instrument equipped with an APEX II CCD area detector fixed at a distance of 5.0 cm from the crystal and a Cu Kα fine focus sealed tube (λ = 1.54178 nm) operated at 1.5 kW (50 kV, 30 mA), filtered with a graphite monochromator. All diffraction data were processed with the Bruker Apex II software suite. Selected data are shown in Table S2.

Identification code	1	2	3
Empirical formula	$C_{28}H_{22}$	$C_{28}H_{22}O_{0.25}$	C_7H_4O
Formula weight	358.45	362.45	104.10
Temperature/K	296(2)	296(2)	296(2)
Crystal system	monoclinic	monoclinic	monoclinic
Space group	$P2_1/n$	C2/c	$P2_1/c$
a/Å	12.5501(12)	22.3284(6)	7.8768(2)
b/Å	5.8657(6)	7.7485(2)	3.97070(10)
c/Å	12.8898(13)	13.6688(3)	15.8098(3)
α/°	90	90	90
β/°	95.234(6)	126.7290(10)	102.6710(10)
γ/°	90	90	90
Volume/Å^3	944.93(16)	1895.37(8)	482.43(2)

Crystal structure of compound 1 (9,9′,10,10′-tetrahydro-9,9′-bianthracene)

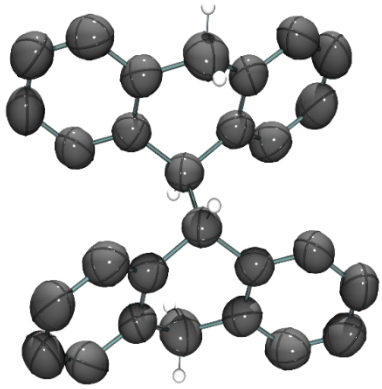

Figure S14. Crystal structure of **1** (50 % ellipsoids). All hydrogen atoms are omitted for clarity other than hydrogen on sp^3 carbon. Color scheme: gray = C, white = H, and red = O. Crystal parameters matched those reported elsewhere.[3,4]

Crystal structure of compound 2 (bianthronyl)

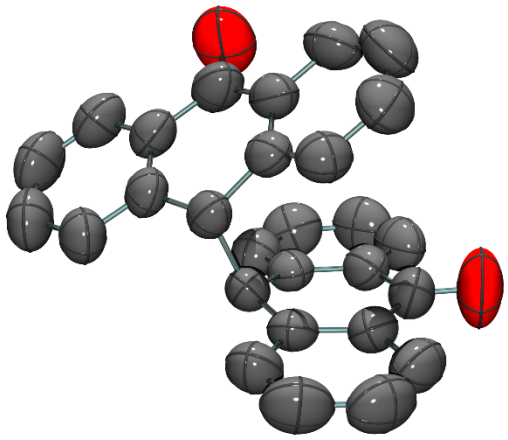

Figure S15. Crystal structure of **2** (50 % ellipsoids). All hydrogen atoms are omitted for clarity. Color scheme: gray = C and red = O. Crystal parameters matched those reported elsewhere.[5]

Crystal structure of compound 3 (anthraquinone)

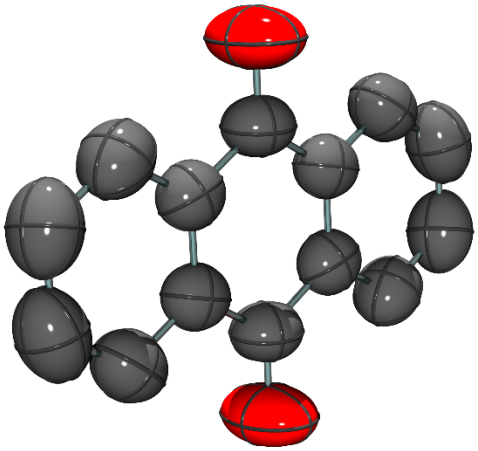

Figure S16. Crystal structure of **3** (50 % ellipsoids). All hydrogen atoms are omitted for clarity. Color scheme: gray = C and red = O. Crystal parameters matched those reported elsewhere.[6]

^{1}H NMR spectra for the reaction of toluene with $V^V(O)(O)$ under air and N_2

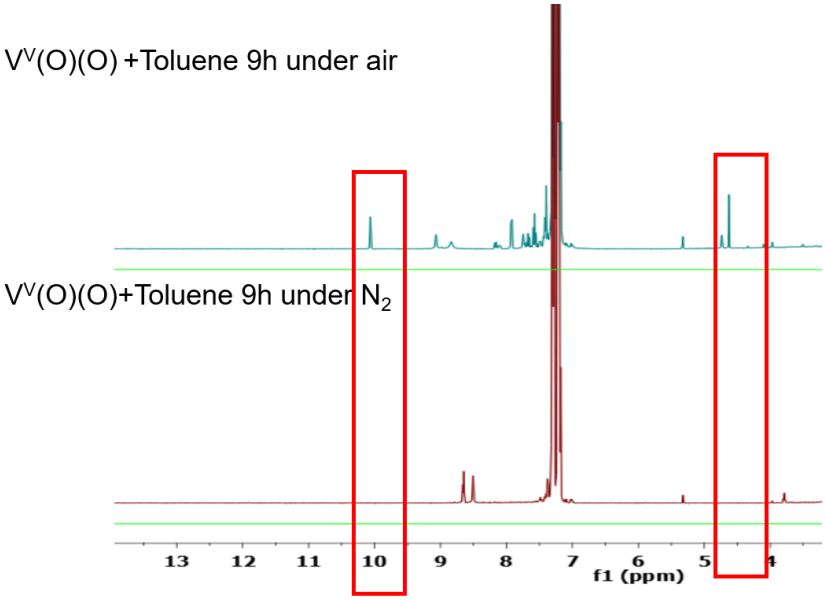

Figure S17. ^{1}H NMR spectra for reaction with toluene in CD_3CN under air (top) and N_2 (bottom) (540 min irradiation for both cases).

^{1}H NMR spectra for reaction of DHA with $V^V(O)(O)$ under air and N_2

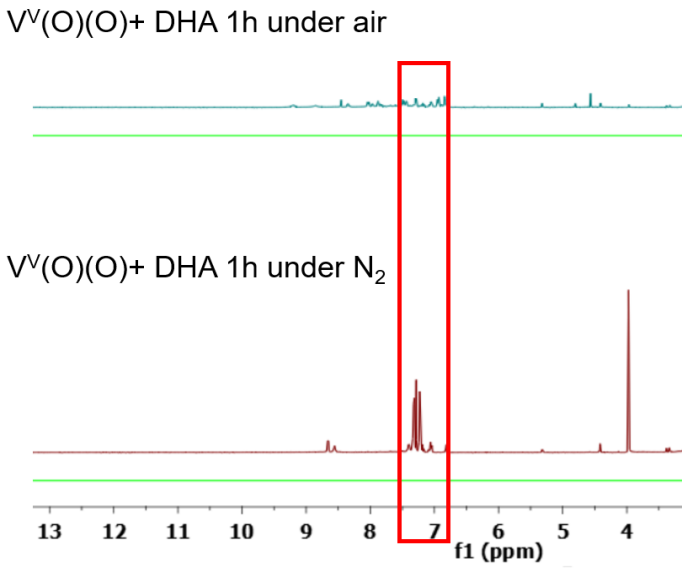

Figure S18. ^{1}H NMR spectra for reaction with DHA in CD_3CN under air (top) and N_2 (bottom) (60 min irradiation for both cases).

Comparison of photochemical oxidations using different ratios of V-complexes and DHA under N_2 and O_2

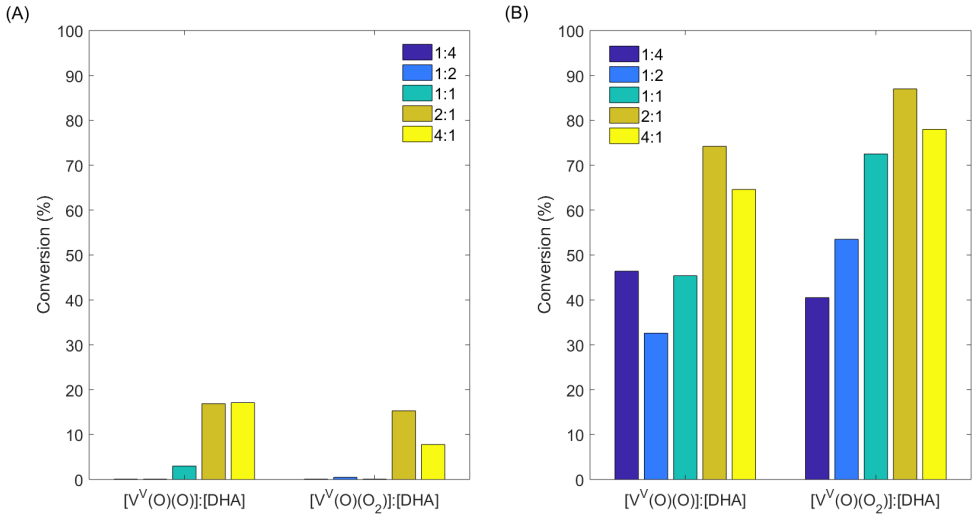

Figure S19. The conversion versus different ratios of $V(O)(O)^tBu/V(O)(O_2)^tBu$ and DHA under N_2 (A) and air (B). In all cases, irradiation time was 60 min.*Note: Figures S19-S28 involve reactions of vanadium complexes in the absences of substrate All reactions times were 60 minutes.*

^{51}V NMR spectra for $V^{V}(O)(O)$ before and after irradiation under O_2, air and N_2

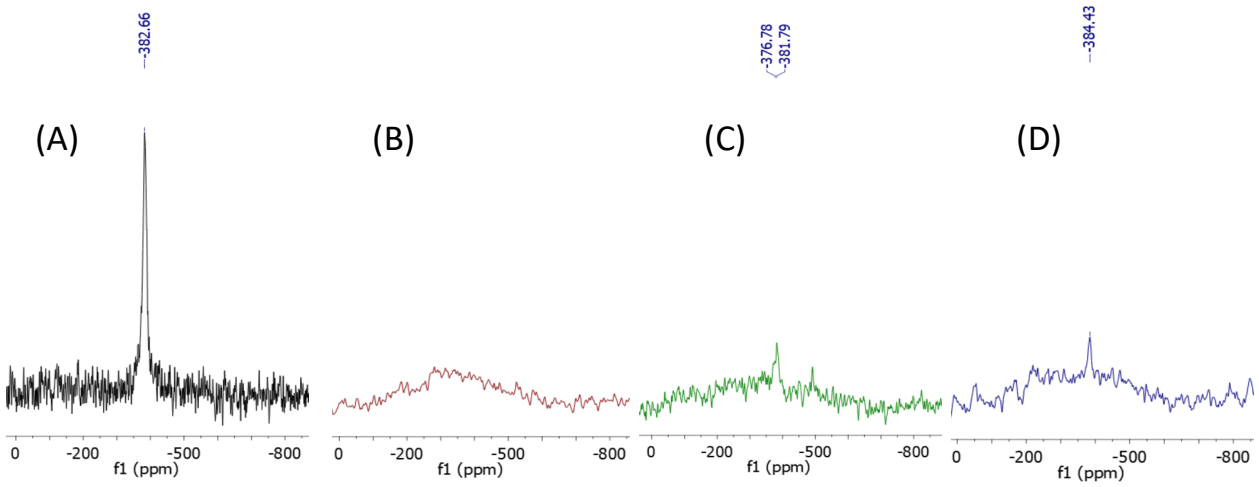

Figure S20. ^{51}V NMR spectra for $V^{V}(O)(O)$ in CD_3CN. (A) Before photochemical reaction; (B) Under air after reaction; (C) Under O_2 after reaction; (D) Under N_2 after reaction.

^{51}V NMR spectra for $V^{V}(O)(O_2)$ before and after photochemical reaction under O_2, air and N_2

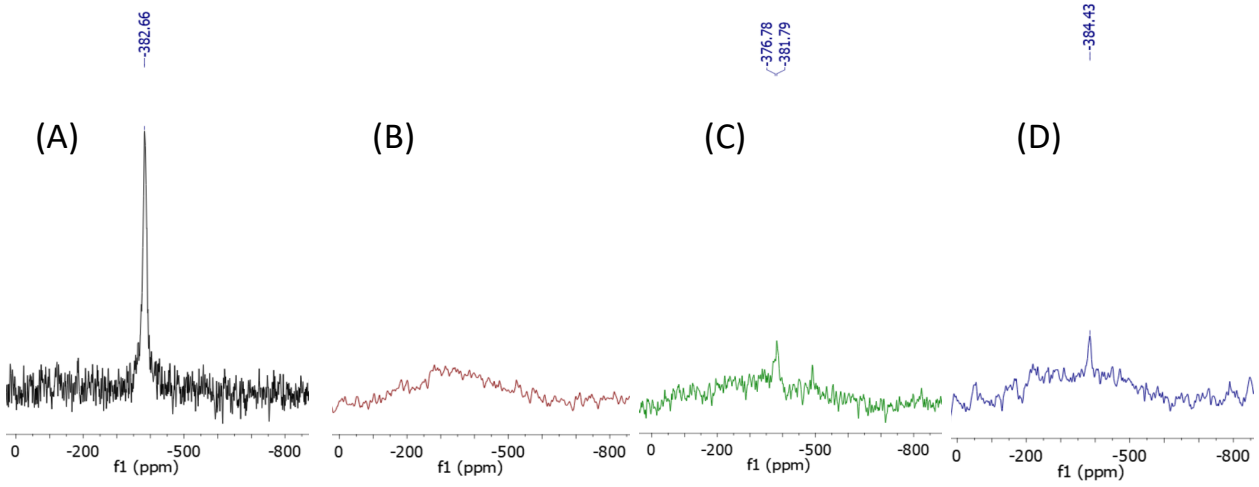

Figure S21. ^{51}V NMR spectra for $V^{V}(O)(O_2)$ in CD_3CN. (A) Before photochemical reaction; (B) Under air after reaction; (C) Under O_2 after reaction; (D) Under N_2 after reaction.

^{1}H NMR spectra for $V^V(O)(O)$ before and after photochemical reaction under O_2, air and N_2

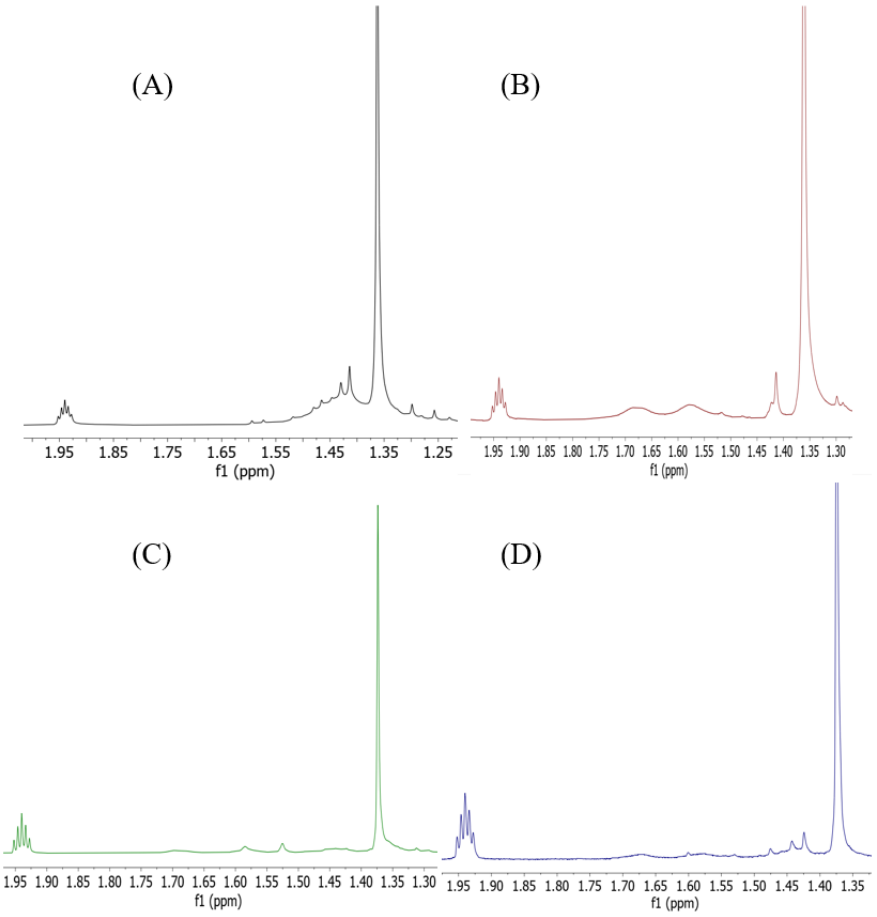

Figure S22. ^{1}H NMR spectra for $V^V(O)(O)$ in CD_3CN. (A) Before photochemical reaction; (B) Under air after reaction; (C) Under O_2 after reaction; (D) Under N_2 after reaction.

^{1}H NMR spectra for $V^V(O)(O_2)$ before and after photochemical reaction under O_2, air and N_2

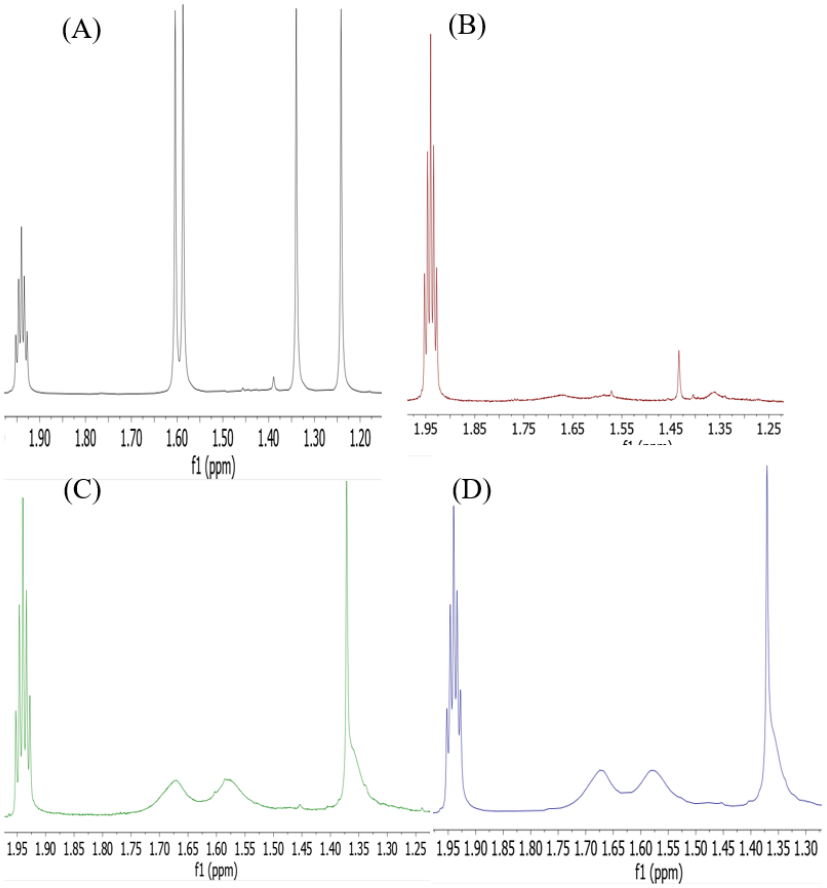

Figure S23. ^{1}H NMR spectra for $V^V(O)(O_2)$ in CD_3CN. (A) Before photochemical reaction; (B) Under air after reaction; (C) Under O_2 after reaction; (D) Under N_2 after reaction.

IR spectra for $V^{IV}(O)(OH)$, $V^{V}(O)(O)$ and $V^{V}(O)(O_2)$

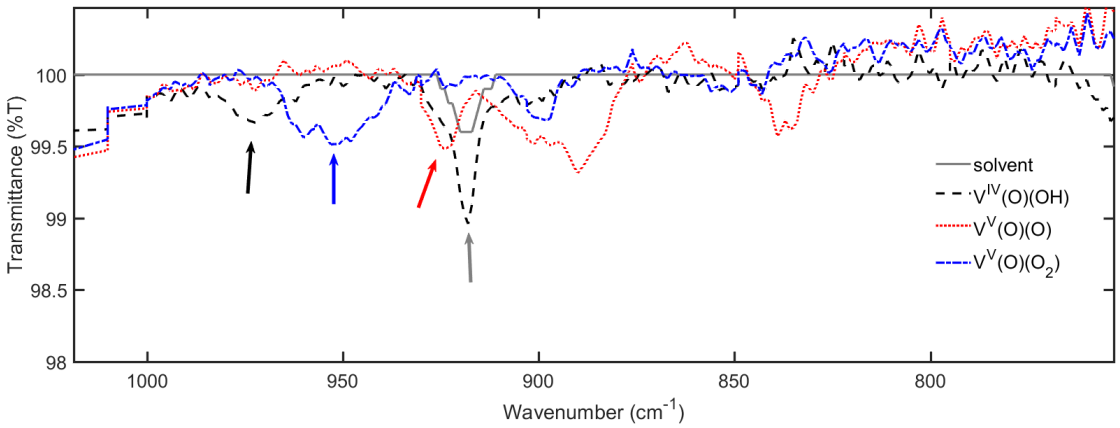

Figure S24. IR spectra for $V^{IV}(O)(OH)$, $V^{V}(O)(O)$ and $V^{V}(O)(O_2)$ in CH_3CN. The V – O stretch for $V^{IV}(O)(OH)$, $V^{V}(O)(O)$ and $V^{V}(O)(O_2)$ were about 969, 925 and 950 cm^{-1}, respectively.

IR spectra for $V^{V}(O)(O)$ before and after photochemical reaction under O_2, air and N_2

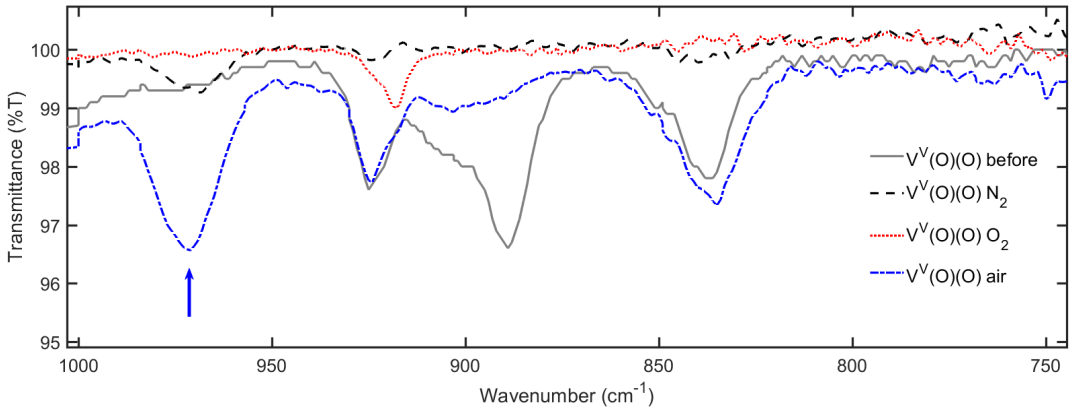

Figure S25. IR spectra for $V^{V}(O)(O)$ before and after photochemical reaction under O_2, air and N_2 in CH_3CN.

IR spectra for $V^{V}(O)(O_2)$ before and after photochemical reaction under O_2, air and N_2

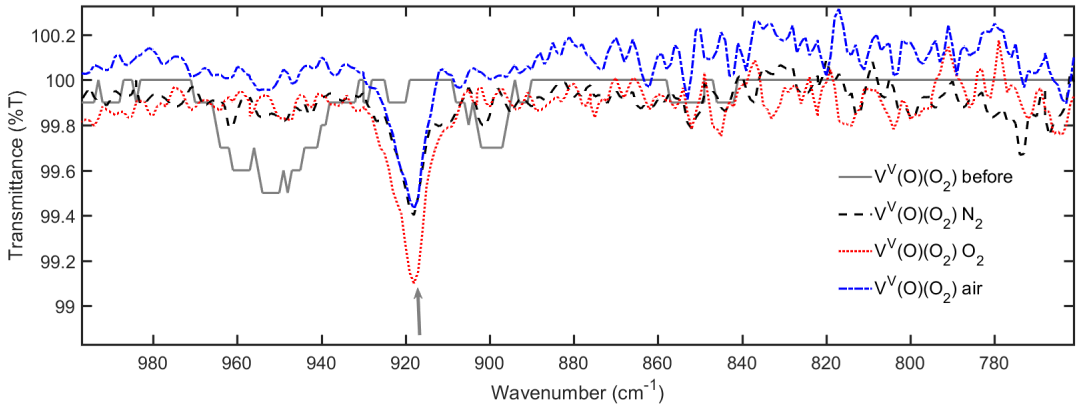

Figure S26. IR spectra for $V^{V}(O)(O_2)$ before and after photochemical reaction under O_2, air and N_2 in CH_3CN.

UV-vis spectra for $V^{IV}(O)(OH)$, $V^{V}(O)(O)$ and $V^{V}(O)(O_2)$

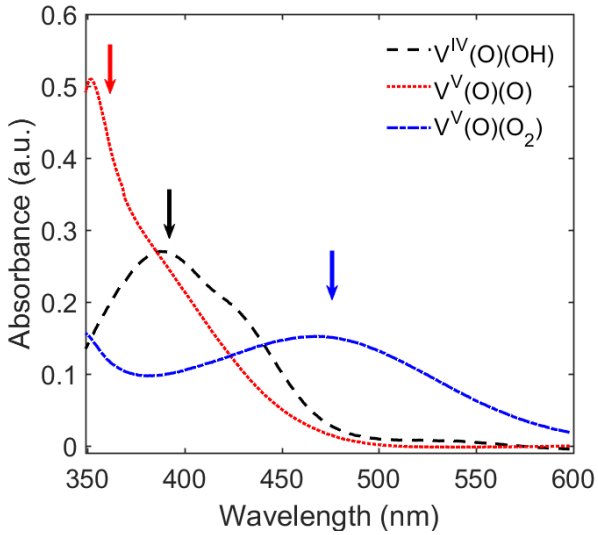

Figure S27. UV-vis spectra for $V^{IV}(O)(OH)$, $V^{V}(O)(O)$ and $V^{V}(O)(O_2)$ in CH_3CN. The absorption for $V^{IV}(O)(OH)$, $V^{V}(O)(O)$ and $V^{V}(O)(O_2)$ were about 390, 360 and 475 nm, respectively.

UV-vis spectra for $V^{V}(O)(O)$ before and after photochemical reaction under O_2, air and N_2

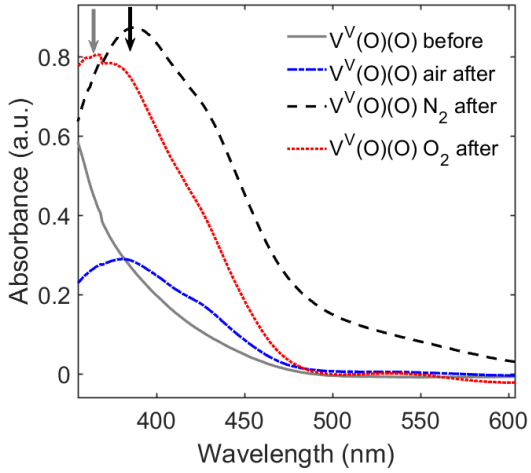

Figure S28. UV-vis spectra for $V^{V}(O)(O)$ before and after photochemical reaction under O_2, air and N_2 in CH_3CN.

UV-vis spectra for $V^{V}(O)(O_2)$ before and after photochemical reaction under O_2, air and N_2

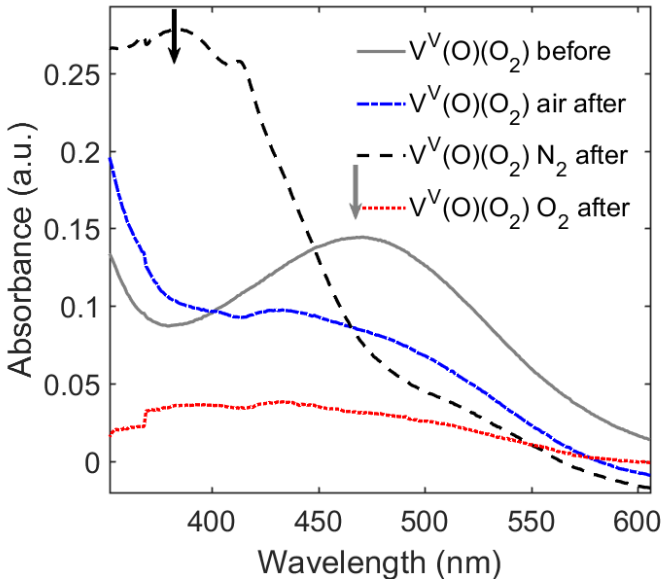

Figure S29. UV-vis spectra for $V^{V}(O)(O_2)$ before and after photochemical reaction under O_2, air and N_2 in CH_3CN.

Computational Details

Calculations were performed using the ORCA 4.2.1 *ab initio* quantum chemistry program.[7,8] Geometry optimizations and single point calculations were carried out using the TPSSh functional, utilizing the RIJCOSX algorithm.[9] The basis set was def2-TZVP(-f)/def2/J [10–12] and the Becke-Johnson damping scheme[13,14] on all atoms. The optimized structure were characterized using vibrational frequency calculations at the same level of theory to confirm that the structures were located at a minimum on the potential energy surface. Metrical parameters calculated for cis-V(O)(O)(4,4′-dimethylbipyridyl)$^+$ are similar to those in an experimental X-ray structure.[1] TD-DT For direct comparison with TD-DFT calculations, single-point energy calculations used the TPSS[15] functional and def2-TZVP(-f) def2-TZVP/C basis set[10–12] in acetonitrile solvent using the a dielectric continuum model (CPCM).[16]

Coordinates for the optimized geometry of cis-V(O)(O)(4,4′-dimethylbipyridyl)$^+$

V	6.11941896773942	-0.45497842799425	3.17792006162757
O	7.42171822791517	0.23419708693504	3.86243064469444
O	6.65719097869000	-1.33642884485130	1.92568235155056
N	4.90224421813376	0.20495097743733	5.00593609921729
N	5.86680993267706	-2.15956357626153	4.41219124184775
N	5.59842040115707	1.28724768358628	2.09684091518601
N	3.94659965808749	-0.71658254645268	2.45953161097691
C	4.45331742695137	1.44126138659987	5.24301677471115
H	4.55686894493672	2.15638250989757	4.43685147531889
C	3.88177309989034	1.81700556961199	6.45017516511002
H	3.53235847962820	2.83382548579273	6.57910038850640
C	3.76555004642875	0.88260017728372	7.47868161441956
C	3.17191589502349	1.23169622560776	8.81227298886765
C	4.23524915805885	-0.40633581426814	7.22273530428836
H	4.16410983024288	-1.16372569386770	7.99205479390295
C	4.79373627190739	-0.71246390423155	5.98763644167676
C	5.30848029449492	-2.04854263543925	5.64286968173848
C	5.22302256403763	-3.14193344774523	6.49295071223675
H	4.76732605086169	-3.02885337046565	7.46749181117825
C	5.71069817625889	-4.38915485856112	6.09913448395671
C	5.63818005727617	-5.57167189933142	7.01733407871840
C	6.26840371438234	-4.48106495991579	4.82411739003691
H	6.65625235425533	-5.42017760211314	4.45051916537879
C	6.33099818220032	-3.35797662742191	4.01934778166465
H	6.75786610467339	-3.39417972947902	3.02665613159933
C	6.50832691900401	2.26516780156075	1.93586676410267
H	7.40346949084912	2.17671399377596	2.53529399130056
C	6.32298626480415	3.31382859135832	1.05688718228515
H	7.09219703746401	4.07043477005487	0.96823643051088
C	5.15654928616686	3.37762011981659	0.29066339086914
C	4.94565516708622	4.46753963124754	-0.71530720005892
C	4.20979895419081	2.37326547693818	0.48471605219002
H	3.28769584917825	2.39084285286609	-0.08011213049193
C	4.44673079857131	1.34428309425520	1.38820613786388
C	3.49165760480615	0.25239442965249	1.64241305705319
C	2.21071685355333	0.21725914403950	1.09656135295604
H	1.87227101327832	1.01493385530226	0.44890095863973
C	1.35098681052311	-0.83783910057734	1.39387454612903

C	-0.04047505532337	-0.90127360638836	0.83569190376245
C	1.84206559650787	-1.83784362811795	2.23695964165054
H	1.22988066516078	-2.68838466149653	2.51083784221371
C	3.12980964585105	-1.74097343613457	2.73661384486284
H	3.52296814893012	-2.51187841187625	3.38557366452571
H	2.73493196267835	2.23009194271820	8.80176900979656
H	3.94508268008313	1.19678393794816	9.58507099940136
H	2.40175192396629	0.50890977548609	9.09012220136003
H	5.94782491806296	-6.48434213621923	6.50935774886174
H	4.62293374777036	-5.69930508354470	7.40025593584026
H	6.29195709798322	-5.41170489880348	7.87949093445543
H	-0.26412944995417	-0.02555203344425	0.22687575219766
H	-0.77061178649273	-0.96437134836633	1.64667260558404
H	-0.16132063317417	-1.79695038277863	0.22053597448694
H	3.89792628828449	4.54438512279118	-1.00576822757744
H	5.53394736760948	4.25100272709856	-1.61275052690357
H	5.28709579667204	5.42659829648508	-0.32209894627820

Positions of the 25 lowest energy transitions for cis-V(O)(O)(4,4′-dimethylbipyridyl)$^+$

State	Energy (cm^{-1})	Wavelength (nm)	fosc	P2 (au**2)	PX (au)	PY (au)	PZ (au)
1	19525.8	512.1	0.004701750	0.07927	-0.08012	0.17069	-0.20910
2	20625.0	484.8	0.003301317	0.05269	-0.17988	-0.03603	0.13799
3	25287.2	395.5	0.000291920	0.00380	-0.02163	-0.02164	0.05352
4	26332.6	379.8	0.000981599	0.01227	-0.09759	0.04195	-0.03143
5	26729.3	374.1	0.002189815	0.02697	-0.11418	0.00941	0.11767
6	28220.0	354.4	0.002184316	0.02548	-0.05093	0.14499	-0.04321
7	28459.5	351.4	0.000517156	0.00598	0.00659	0.00759	0.07669
8	28588.4	349.8	0.002848295	0.03280	-0.07702	-0.14139	0.08292
9	29340.5	340.8	0.000489106	0.00549	-0.00819	-0.03346	0.06558
10	29861.2	334.9	0.000536629	0.00592	-0.06927	0.00719	0.03266
11	30249.3	330.6	0.003523602	0.03835	-0.03512	0.13285	-0.13952
12	30807.1	324.6	0.047476397	0.50734	0.15695	-0.37109	0.58737
13	31333.1	319.2	0.001524425	0.01602	-0.00265	-0.10897	0.06430
14	31502.9	317.4	0.001837386	0.01920	-0.04504	0.08939	-0.09583
15	31938.4	313.1	0.002203794	0.02272	0.06619	0.12029	0.06217
16	32448.4	308.2	0.113834510	1.15493	-0.92003	-0.52043	0.19397
17	32558.3	307.1	0.074583895	0.75415	-0.20047	0.77142	0.34479
18	32699.4	305.8	0.044332078	0.44633	-0.05807	0.64027	0.18170
19	33679.5	296.9	0.025790035	0.25209	0.32184	-0.29485	0.24815
20	33998.7	294.1	0.012935776	0.12526	0.13213	0.09858	-0.31318
21	34043.2	293.7	0.009771047	0.09449	-0.24317	-0.18742	-0.01527
22	34118.1	293.1	0.021674506	0.20914	0.11466	0.08637	-0.43421
23	34587.9	289.1	0.020394524	0.19412	-0.20396	0.35140	0.17040
24	34736.1	287.9	0.004407933	0.04178	0.19852	0.00719	0.04810
25	35221.4	283.9	0.001709609	0.01598	0.11510	-0.05221	0.00238

References

(1) Waidmann, C. R.; Zhou, X.; Tsai, E. A.; Kaminsky, W.; Hrovat, D. A.; Borden, W. T.; Mayer, J. M. Slow Hydrogen Atom Transfer Reactions of Oxo- and Hydroxo-Vanadium Compounds: The Importance of Intrinsic Barriers. *J. Am. Chem. Soc.* **2009**, *131*, 4729–4743. https://doi.org/doi: 10.1021/ja808698x.

(2) Waidmann, C. R.; DiPasquale, A. G.; Mayer, J. M. Synthesis and Reactivity of Oxo-Peroxo-Vanadium(V) Bipyridine Compounds. *Inorg. Chem.* **2010**, *49* (5), 2383–2391. https://doi.org/10.1021/ic9022618.

(3) Li, P.-C.; Wang, T.-S.; Lee, G.-H.; Liu, Y.-H.; Wang, Y.; Chen, C.-T.; Chao, I. Theoretical Study and X-Ray Determination of Bianthrones: Long C−C Bond Length and Preferred Gauche Conformation. *J. Org. Chem.* **2002**, *67* (23), 8002–8009. https://doi.org/10.1021/jo020196g.

(4) Li, P.-C.; Wang, T.-S.; Lee, G.-H.; Liu, Y.-H.; Wang, Y.; Chen, C.-T.; Chao, I. Theoretical Study and X-Ray Determination of Bianthrones: Long C−C Bond Length and Preferred Gauche Conformation. *J. Org. Chem.* **2003**, *68* (6), 2528–2528. https://doi.org/10.1021/jo0399246.

(5) Wen, Z.-G.; Li, J.-M. Redermination of 9,9′-Bianthracene-10,10′(9H,9′H)-Dione. *Acta Cryst E* **2008**, *64* (10), o1931–o1931. https://doi.org/10.1107/S1600536808028833.

(6) Lonsdale, K.; Milledge, J.; El Sayed, K. The Crystal Structure (at Five Temperatures) and Anisotropic Thermal Expansion of Anthraquinone. *Acta Cryst* **1966**, *20* (1), 1–13. https://doi.org/10.1107/S0365110X6600001X.

(7) Neese, F. The ORCA Program System. *WIREs: Comput. Mol. Sci.* **2012**, *2*, 73–78.

(8) Neese, F. Software Update: The ORCA Program System, Version 4.0. *WIREs: Comput. Mol. Sci.* **2018**, *8* (1), e1327. https://doi.org/10.1002/wcms.1327.

(9) Neese, F.; Wennmohs, F.; Hansen, A.; Becker, U. Efficient, Approximate and Parallel Hartree–Fock and Hybrid DFT Calculations. A 'Chain-of-Spheres' Algorithm for the Hartree–Fock Exchange. *Chem. Phys.* **2009**, *356* (1), 98–109. https://doi.org/10.1016/j.chemphys.2008.10.036.

(10) Weigend, F. Accurate Coulomb-Fitting Basis Sets for H to Rn. *Phys. Chem. Chem. Phys.* **2006**, *8* (9), 1057–1065. https://doi.org/10.1039/B515623H.

(11) Weigend, F.; Ahlrichs, R. Balanced Basis Sets of Split Valence, Triple Zeta Valence and Quadruple Zeta Valence Quality for H to Rn: Design and Assessment of Accuracy. *Phys. Chem. Chem. Phys.* **2005**, *7* (18), 3297–3305. https://doi.org/10.1039/B508541A.

(12) Hellweg, A.; Hättig, C.; Höfener, S.; Klopper, W. Optimized Accurate Auxiliary Basis Sets for RI-MP2 and RI-CC2 Calculations for the Atoms Rb to Rn. *Theor Chem Acc* **2007**, *117* (4), 587–597. https://doi.org/10.1007/s00214-007-0250-5.

(13) Grimme, S.; Antony, J.; Ehrlich, S.; Krieg, H. A Consistent and Accurate Ab Initio Parametrization of Density Functional Dispersion Correction (DFT-D) for the 94 Elements H-Pu. *J. Chem. Phys.* **2010**, *132* (15), 154104. https://doi.org/10.1063/1.3382344.

(14) Grimme, S.; Ehrlich, S.; Goerigk, L. Effect of the Damping Function in Dispersion Corrected Density Functional Theory. *J. Comput. Chem.* **2011**, *32* (7), 1456–1465. https://doi.org/10.1002/jcc.21759.

(15) Tao, J.; Perdew, J. P.; Staroverov, V. N.; Scuseria, G. E. Climbing the Density Functional Ladder: Nonempirical Meta--Generalized Gradient Approximation Designed for Molecules and Solids. *Phys. Rev. Lett.* **2003**, *91* (14), 146401. https://doi.org/10.1103/PhysRevLett.91.146401.

(16) Cossi, M.; Rega, N.; Scalmani, G.; Barone, V. Energies, Structures, and Electronic Properties of Molecules in Solution with the C-PCM Solvation Model. *J. Comput. Chem.* **2003**, *24* (6), 669–681. https://doi.org/10.1002/jcc.10189.